R AUTHORITY
of Western Australia

WATER RESOURCES DIRECTORATE

NUMERICAL MODELS TO SIMULATE WATER MOVEMENT IN VERTICAL, SLOPING AND LAYERED SOILS

Report No. WH 13
February 1986

WATER AUTHORITY
of Western Australia

WATER RESOURCES DIRECTORATE

Hydrology Branch

NUMERICAL MODELS TO SIMULATE WATER MOVEMENT IN VERTICAL, SLOPING AND LAYERED SOILS

N.J. Schofield

Report No. WH 13
February 1986

ABSTRACT

The development and operation of two numerical soil water models are described. The first model is restricted to one-dimensional vertical water movement and incorporates the processes of infiltration, redistribution and soil water evaporation. The second model represents a uniform slope with parallel soil horizons, and includes the additional processes of overland flow and saturated throughflow. The general approach adopted was to simulate flow for periods of several months without undue reduction in the representation of physical processes.

Three soil textural classes were considered: gravelly sand, sandy loam and clay. Measured rainfall and evaporation data were input to the model. The depth of infiltration was found to be strongly dependent on textural class, and to a lesser extent, on initial water content. Soil water evaporation was significantly smaller for the more permeable gravelly sand. In the slope simulation, duplex soils with an impeding clay subsoil formed perched water tables and, when the upper aquifer became saturated, produced overland flow. The amount of overland flow depended strongly on the initial soil water deficit and hydraulic conductivity of the upper aquifer.

CONTENTS

Figure Captions

Figure 1 One dimensional vertical soil water model

Figure 2a Water desorption curves of three major soils of Wights catchment, Western Australia (after Sharma et al. 1980)

Figure 2b Calculated hydraulic conductivity as a function of water content for three major soils of Wights catchment, Western Australia (after Sharma et al. 1980)

Figure 3 Conductivity weighting for compartment boundaries

Figure 4 Top layer evaporation characteristics for different soil textures

Figure 5 Rainfall and Class A pan evaporation, June-September 1979, from Waroona, Western Australia

Figure 6 Soil water profiles following infiltration and ponding on clay

Figure 7 Soil water profiles following infiltration into yellow earths for various initial water profiles

Figure 8 Soil water profiles following infiltration into gravelly sand for various initial water profiles

Figure 9 Soil water profile time series showing infiltration, redistribution and evaporation in gravelly sand

Figure 10 Schematic diagram of one-dimensional uniform slope model

Figure 11 Clay uniform slope simulation showing overland flow and soil water profile responses to rainfall

List of Tables

1. INTRODUCTION

The advent of computers as a research tool in the 1950's led to many advances in the numerical modelling of individual physical processes of soil water dynamics. Since that time numerical studies of infiltration, redistribution and evaporation have been undertaken for various soil conditions (e.g. Klute, 1952; Whisler et al., 1972; Wind and Van Doorne, 1975; Hillel, 1975; Haverkamp et al., 1977). Such intricate problems as hysteresis (Rubin, 1967; Watson and Lees, 1975), air pressure effects (Vachaud et al., 1973; Watson and Curtis, 1975), layered profiles (Hanks and Bowers, 1962; Hillel and Talpaz, 1977) and spatial variability (Dagan and Bresler, 1983; Clapp, 1983) have also been addressed. Although more detailed research on individual processes is undoubtedly required, the aim of the modelling presented here is to simulate seasonal soil water dynamics in Western Australian soils without undue loss of physical detail.

Two models were developed to examine vertical and lateral water movement in soils commonly found in the south-west of W.A. Both models treat the soil profile as composed of distinct horizons, with each horizon having uniform properties. Three soil types, namely gravelly sand, yellow earth and clay, for which physical and hydraulic properties have been published (Sharma et al., 1980), were used in the modelling. Various combinations of soil types including uniform profiles and duplex profiles were investigated. Of particular interest were duplex soils consisting of sands or loams overlying a low permeability clay horizon. These profiles are widespread in the ancient lateratized landscape of W.A. They frequently perch water above the impeding clay horizon during winter and generate saturated throughflow, which is considered a major component of stream runoff (Stokes and Loh, 1982).

2. ONE DIMENSIONAL VERTICAL SOIL WATER MODEL

2.1 Mathematical Formulation

Model assumptions

It was assumed that the soil was homogeneous, isotropic and non-swelling; that there was no hysteresis in the soil water characteristic curve and that the movement of water occurred under isothermal conditions. It was recognised that hysteresis would probably be important when both wetting and drying processes were being considered but its inclusion was beyond the scope of this work.

Mathematical model

The soil profile was divided into a fixed number of compartments or layers of constant or variable thickness (Fig. 1). The change in water content (θ) of a given layer with time was determined simply by the continuity equation:

$$\frac{\partial \theta}{\partial t} = - \frac{\partial q}{\partial z} \qquad (1)$$

where t is time, q is the soil water flux and z is depth. The soil water flux was given by Darcy's law:

$$q = - K(\theta) \frac{\partial h}{\partial z} \qquad (2)$$

where $K(\theta)$ is the hydraulic conductivity function and h is the total soil water potential. It was assumed that h comprises solely the soil water pressure head (ψ) and gravitational potential head (z) expressed as depth below the soil surface, viz

$$h = \psi - z \qquad (3)$$

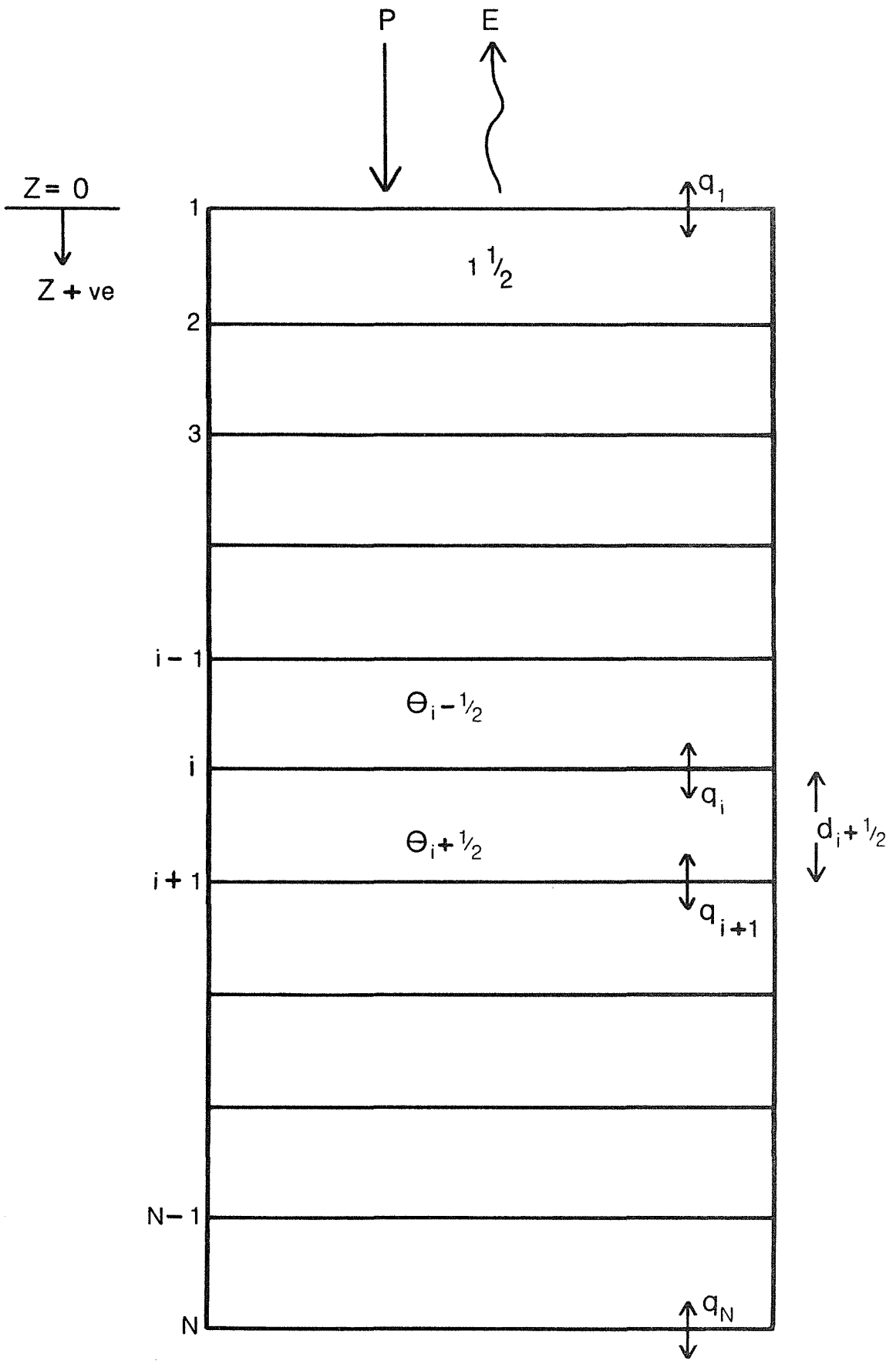

One-dimensional vertical soil water model

FIGURE 1

Substituting equations (2) and (3) into equation (1) gives

$$\frac{\partial \theta}{\partial t} = \frac{\partial}{\partial z}\left[K(\theta) \frac{\partial \psi}{\partial z} \right] + \frac{\partial}{\partial z} K(\theta) \qquad (4)$$

If $\theta_{i+\frac{1}{2}}$ is the water content of the $i+\frac{1}{2}$ layer, with boundary fluxes q_i and q_{i+1} and thickness $d_{i+\frac{1}{2}}$ then the solution of (N-1) first order differential equations of the form:

$$\frac{d\theta}{dt}_{i+\frac{1}{2}} = (q_i - q_{i+1})/d_{i+\frac{1}{2}} \quad , \; i = 1, N-1 \qquad (5)$$

where

$$q_i = -K_i(\theta) \frac{(h_{i+\frac{1}{2}} - h_{i-\frac{1}{2}})}{0.5(d_{i-\frac{1}{2}} + d_{i+\frac{1}{2}})} \qquad (6)$$

is required. The determination of $K(\theta_i)$ is discussed below. A fourth order Runge-Kutta method was employed for the numerical solution (see Appendix I).

At the surface boundary the water flux is the difference between the rainfall input (P) and the evaporation loss (E):

$$q_i = (P - E)/d_{1\frac{1}{2}} \qquad (7)$$

unless the surface layer is saturated in which case ponded infiltration is taken into account.

Soil water pressure head and unsaturated hydraulic conductivity

The soil water pressure head $\psi(\theta)$ and unsaturated hydraulic conductivity $K(\theta)$ functions were taken from published data (Sharma et al., 1980) for a small cleared catchment (Wights) in the

Darling Range of W.A. (Figs. 2a,b). A log-linear fit was made to tabulated data.

Conductivity weighting between layers

To determine the flux across each compartment boundary it is necessary to know the hydraulic conductivity at the boundary. The appropriate value is not easily determined since only conductivity values related to the mean water content of the compartment are known. Haverkamp and Vauclin (1979) tested various approximations to the boundary conductivity for infiltration, including the arithmetic mean, the harmonic mean, the geometric mean and the 'upstream mobility' concept (where the conductivity of the layer which is contributing water is used). Schemes involving the adjacent layer pressure head values and linear interpolation and extrapolation methods were also considered. The authors concluded that the accuracy of the solution for infiltration was very sensitive to the method chosen and that the geometric mean provided the least weighting error. However Markar and Mein (1983) compared different conductivity weighting methods for evaporation from a bare soil and concluded that the upstream mobility method gave the best result. In the present model the upstream mobility method (Fig. 3) was found to give 'smoother' soil water profiles than the geometric mean and was adopted. However it was appreciated that an improved technique should be employed which caters satisfactorily for the combined infiltration, redistribution and evaporation processes. One promising approach is that of Wind and van Doorne (1975) who suggested the integration (analytical or numerical) of fluxes across adjacent layers.

Depth increment

The choice of depth increment, especially near the surface, is known to have a significant influence on predicted evaporation (Markar and Mein, 1983). Increasing the top compartment depth

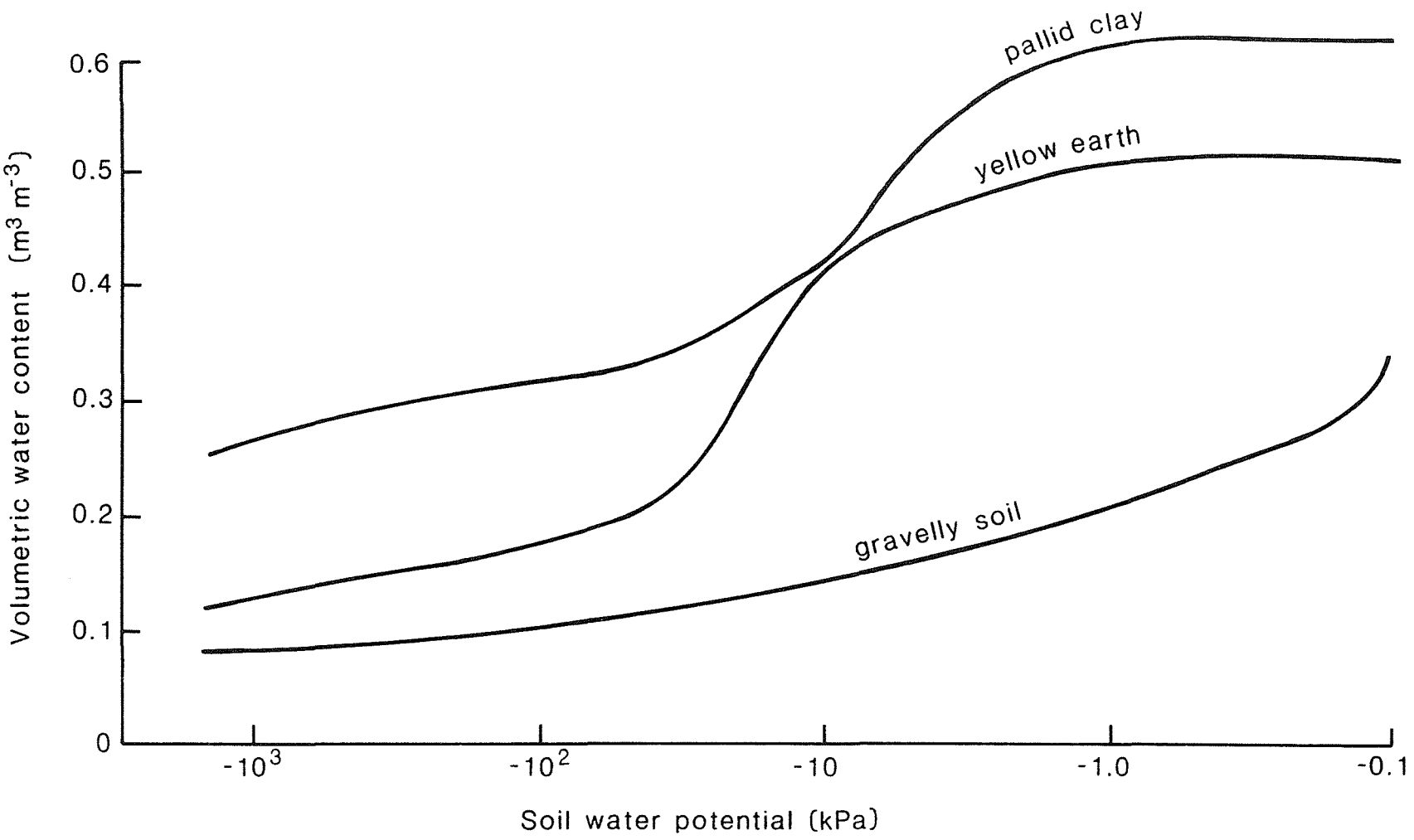

FIGURE 2a

Water desorption curves of three major soils of Wights catchment, Western Australia (after Sharma et al., 1980)

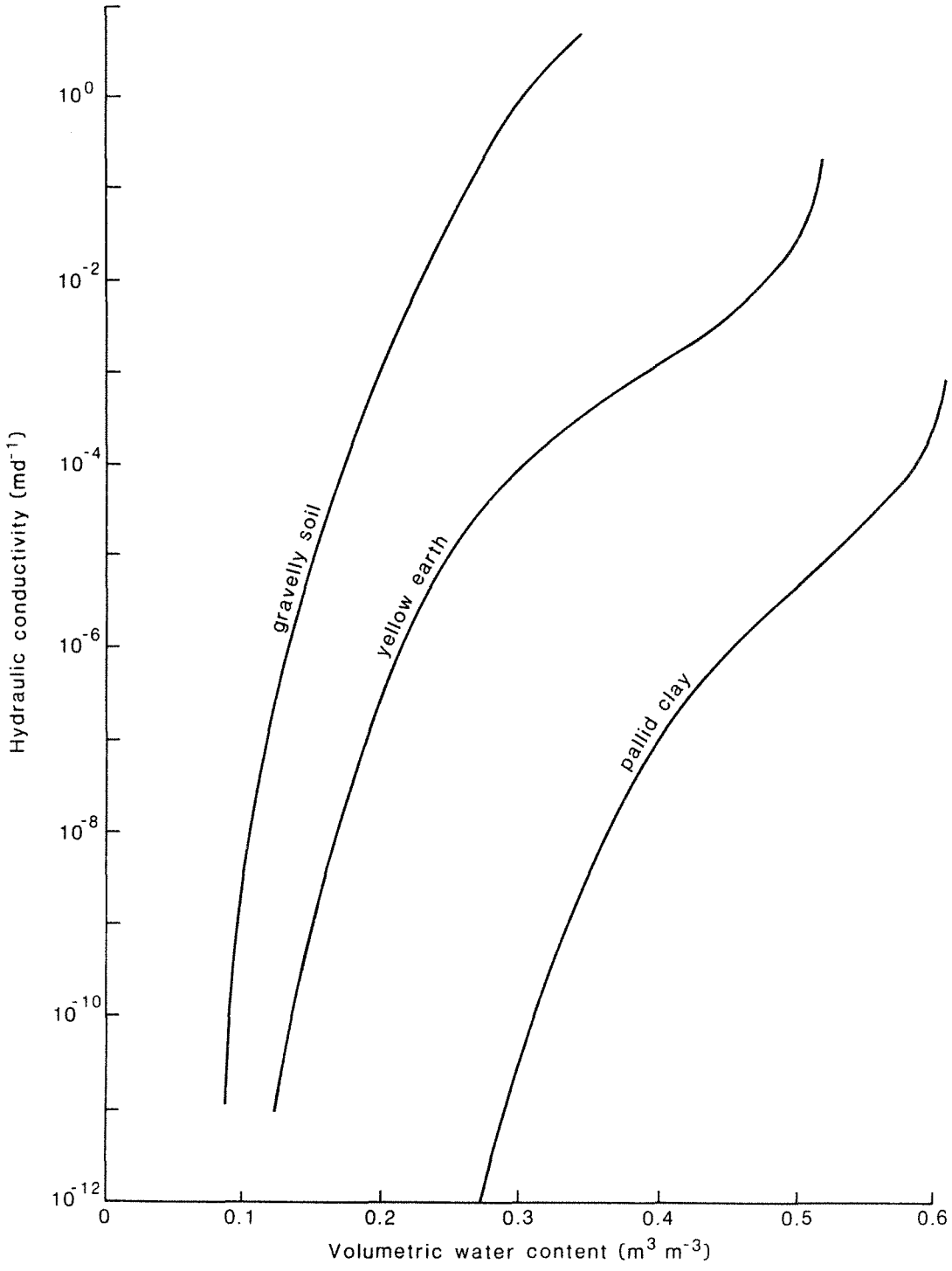

Calculated hydraulic conductivity as a function of water content for three major soils of Wights catchment, Western Australia (after Sharma et al , 1980)

FIGURE 2b

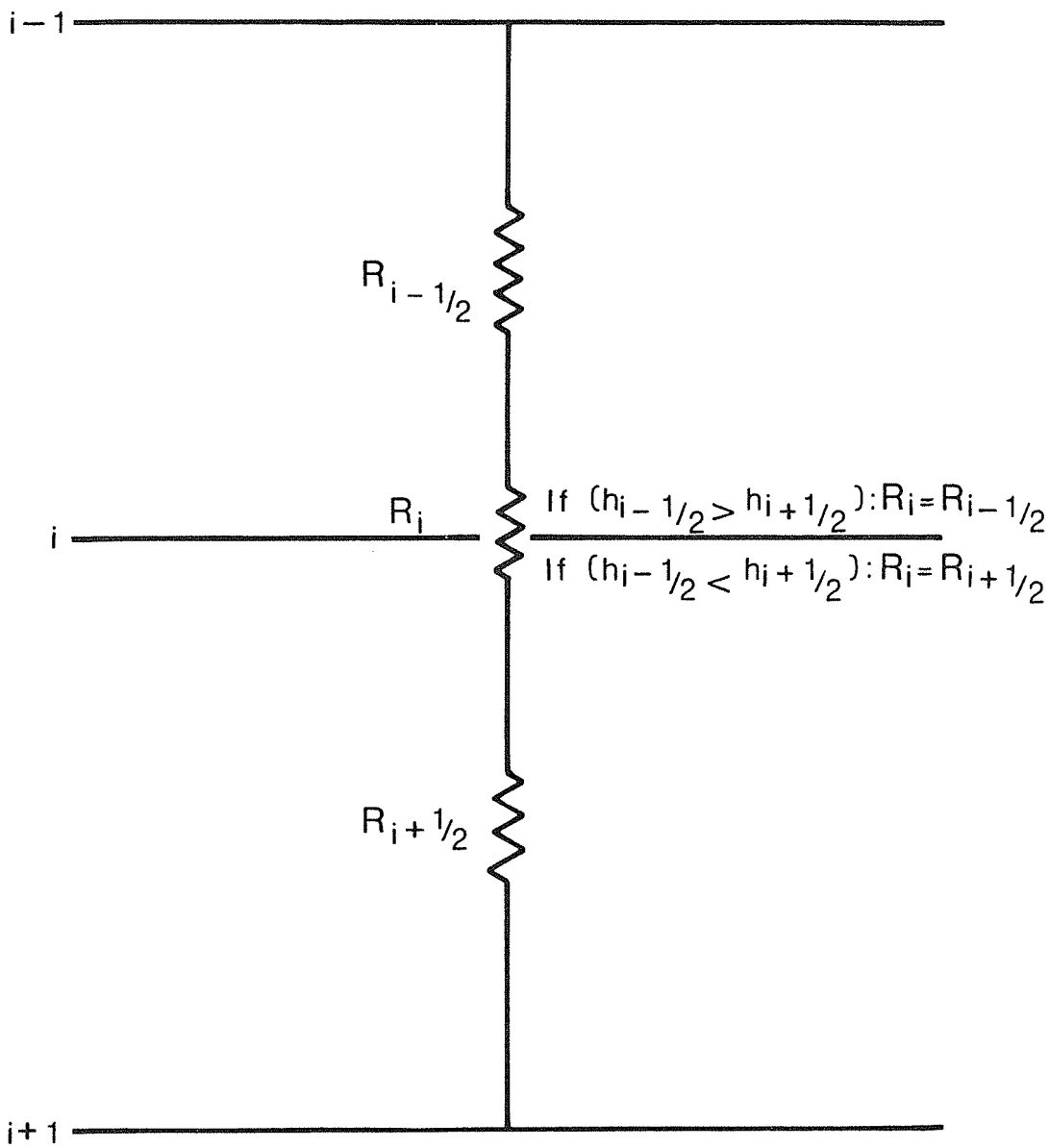

R = flow resistance = inverse of hydraulic conductivity

Conductivity weighting for compartment boundaries

FIGURE 3

increases cumulative evaporation whilst decreasing the depth makes the pressure gradient near the surface much steeper and increases the chance of conductivity weighting errors. In the absence of a preferred method a uniform depth increment was chosen and an evaporation function applied to the uppermost layer which was fitted to different soil types.

Variable time-step

The use of a variable time-step in the solution of the differential equations is extremely useful for both computational efficiency and numerical stability. The criteria used to determine the minimum time-step (Δt) were as follows:

(i) $$\Delta t < \text{minimum} \left| \delta \, d_{i+\frac{1}{2}} / K_{i+\frac{1}{2}} \right|_{i=1,\, N-1} \qquad (8)$$

where δ is an adjustable constant. This criterion essentially ensures that water cannot completely traverse any one compartment in the time-step.

(ii) $$\Delta t < \varepsilon \, d_{1\frac{1}{2}} \, (\theta s_{1\frac{1}{2}} - \theta_{1\frac{1}{2}}) \, / \, P \quad , \; \theta_{1\frac{1}{2}} < \theta s_{1\frac{1}{2}} \qquad (9)$$

where ε is an adjustable constant and $\theta s_{1\frac{1}{2}}$ is the saturated water content of the top layer. This criterion ensured that rainfall did not exceed the current soil water deficit of the top layer within the time interval. This should apply except in the situation where the soil profile itself is becoming or has become saturated, in which case surface ponding or overland flow would be generated.

(iii) $$\Delta t_{max} = \gamma_1 \qquad (10)$$

$$\Delta t_{min} = \gamma_2$$

where γ_1 and γ_2 are adjustable constants defined for each soil type. This criterion setsupper and lower limits for the time-step.

Since rainfall and evaporation data are usually supplied at a fixed time increment, it was necessary to adjust these data to the time-step calculated from the above criteria. The method of doing this is described in Appendix II.

Evaporation

Evaporation was assumed to occur either from water ponded on the soil surface or from water occupying the top soil layer. Evaporation of ponded water simply occurs at the potential evaporation rate (E_p). As regards soil water, the relatively large depth increments used in the model made it necessary to relate the actual evaporation rate (E) to the soil water content of the top layer. To do this a function was devised to closely fit the experimental data of Saxton et al. (1974) for a silt loam soil (Fig. 4). The function utilized the 'end-points' of the soil water evaporation range, that is the saturated water content (θ_s) and the evaporation limit water content (θ_L). [The evaporation limit water content is that water content at which actual evaporation approaches zero]. The function takes the form:

$$E = E_p \exp \left[-c_1 \left(\frac{\theta_s - \theta}{\theta_s - \theta_L} \right)^{c_2} \right] \qquad (11)$$

such that at $\theta = \theta_s$, $E = E_p$.

This equation was applied to the yellow earth soil with the parameters $\theta_s = 0.5$, $\theta_L = 0.25$, $c_1 = 10$, $c_2 = 5$ and the resulting

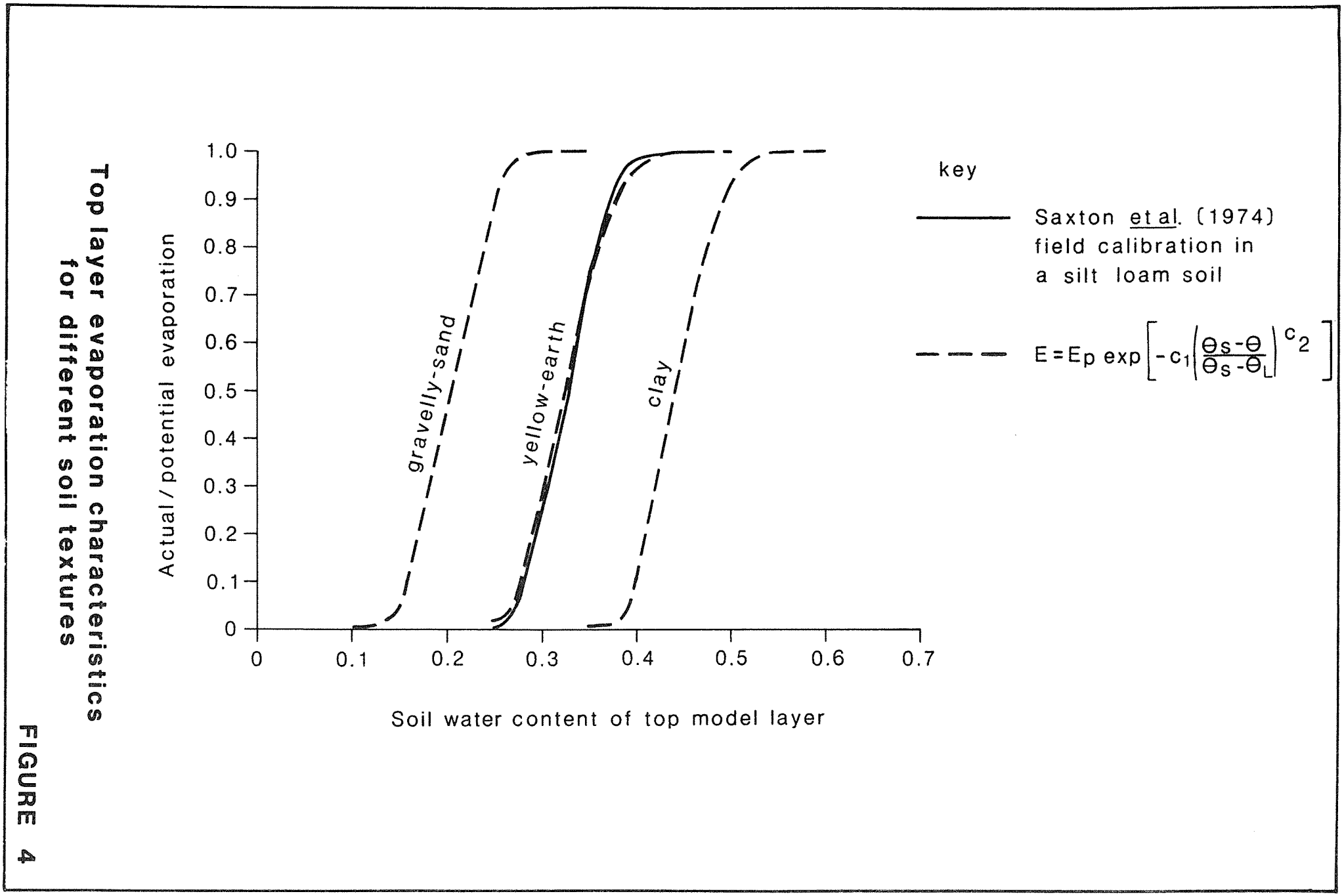

Top layer evaporation characteristics for different soil textures

FIGURE 4

function closely followed the silt loam soil evaporation characteristic in Fig. 4. The sand and clay characteristics in Fig. 4 were predicted using the same c_1 and c_2 parameter values but with their appropriate θ_S and θ_L.

Ponding

The simulation for flat, low permeability soils (e.g. clays) necessarily involves the ponding of water on the soil surface. The effects of ponded water incorporated in the simulation were :

(i) actual evaporation rate is equal to the potential evaporation rate. Within a given time-step, ponded water is evaporated before soil water.

(ii) infiltration occurs under an additional positive head, equal to the depth of the ponded water (H).

Infiltration

In field situations infiltration rate is governed partly by surface conditions and partly by the rate at which water infiltrates deeper into the soil profile. As implied by the model assumptions, only the latter process was included in this model. The reason for the omission of surface factors is the complexity in formulating algorithms to describe such effects as degree of compaction, microbial activity and soil cracking. These factors are probably best dealt with, at least initially, in a detailed surface infiltration model.

2.2 Results

Since the main objective of this modelling exercise was to simulate seasonal water balances, little discussion is given to the short time-scale responses of water content profiles to storm events. The meteorological data input to the model was rainfall

and Class A pan evaporation from Waroona, W.A. for the winter period June-September 1979 (Fig. 5). The total rainfall and potential evaporation for this period were 478 mm and 199 mm respectively. As mentioned previously, three soil types, namely clay, yellow earth and gravelly sand were considered. In each case a uniform initial water content profile or a step increase to saturated water content at depth was assumed (Fig. 6). The soil water properties and model parameters common to all simulations are listed in Table 1. A summary of the initial conditions for all the vertical model simulations is given in Table 2.

Table 1 : Soil water properties and model parameters common to all vertical and slope model simulations

property		values
(time-step criterion constant)		0.01
saturated conductivity (K_{sat})	(clay	0.2×10^{-3} m d^{-1}
	(yellow earth	60.0×10^{-3} m d^{-1}
	(gravelly sand	9.6 m d^{-1}
saturated water content (θ_s)	(clay	0.6 $m^3 m^{-3}$
	(yellow earth	0.5 "
	(gravelly sand	0.35 "
evaporation soil water limit (θ_L)	(clay	0.33 "
	(yellow earth	0.2 "
	(gravelly sand	0.1 "

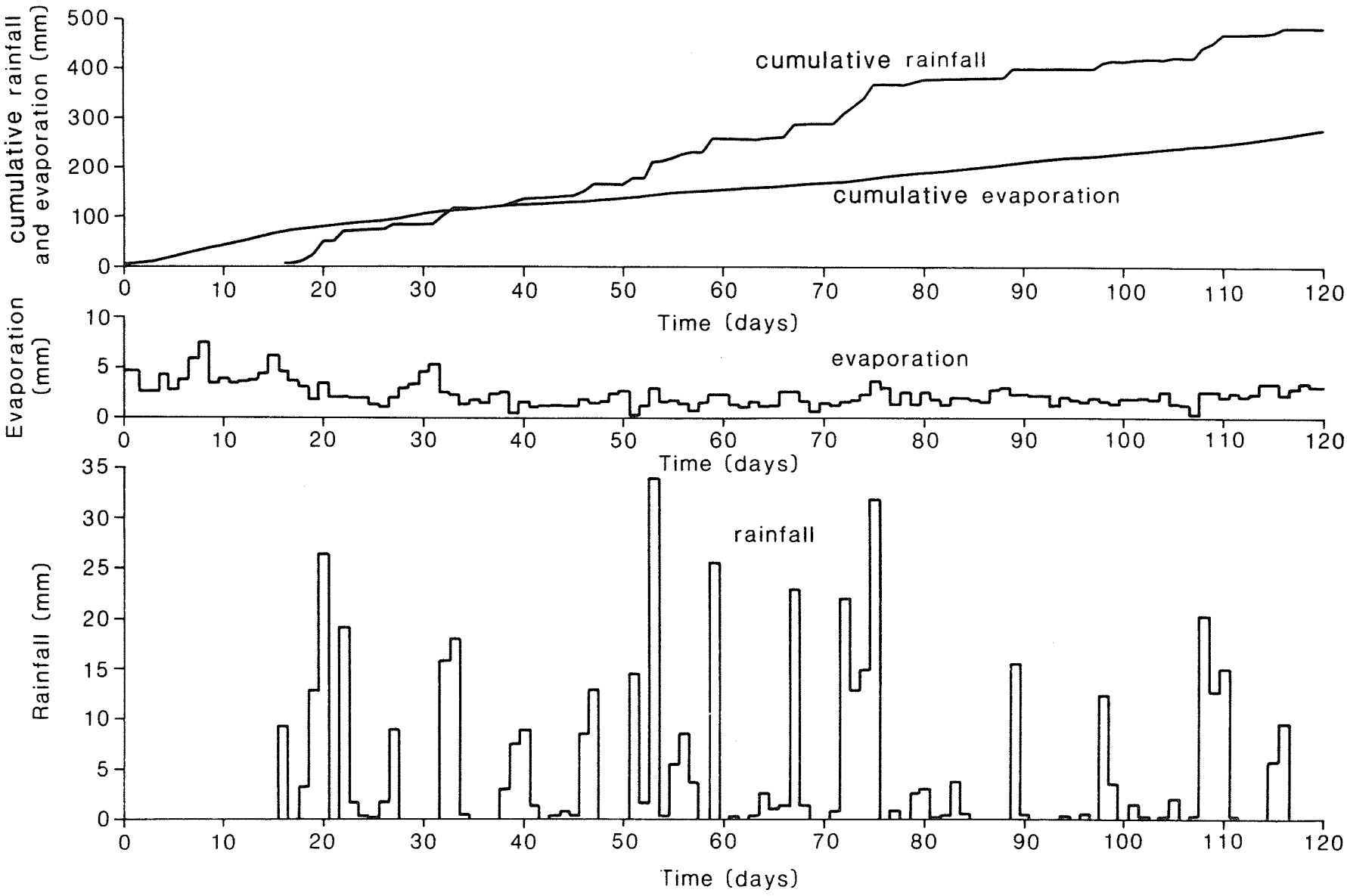

FIGURE 5

Rainfall and class A pan evaporation, June-September 1979, from Waroona, Western Australia

Table 2 : Initial conditions for vertical model simulations

Soil type	Initial water content (m^3m^{-3})	Depth to saturated water (m)	Number of layers	Layer thickness (m)
clay	0.34	1.6	20	0.1
clay	0.55	1.6	20	0.1
yellow earth	0.20	semi-infinte	20	0.25
yellow earth	0.40	4.0	20	0.25
yellow earth	0.40	semi-infinite	20	0.40
gravelly sand	0.11	semi-infinite	20	0.30
gravelly sand	0.20	semi-infinite	20	0.30
gravelly sand	0.11	3.0	10	0.30
gravelly sand	0.20	3.0	10	0.30
gravelly sand	distribution	3.0	10	0.30

Clay

Two initial water contents were considered (θ_{init}= 0.34 and 0.55 m^3m^{-3}) and the resulting soil water profiles for these two cases are shown in Fig. 6. The saturated water at a depth of 1.6 m had no influence on infiltration and redistribution.

In the θ_{init}= 0.34 m^3m^{-3} case, infiltrating water had reached 0.45 m depth by the end of the total period. Ponding of water took place almost immediately and reached a maximum height of 205 mm. Consequently the soil water evaporation (190 mm) was close to the potential evaporation (199 mm). The total change in soil water storage was 89 mm, with 199 mm still ponded at the end of the period.

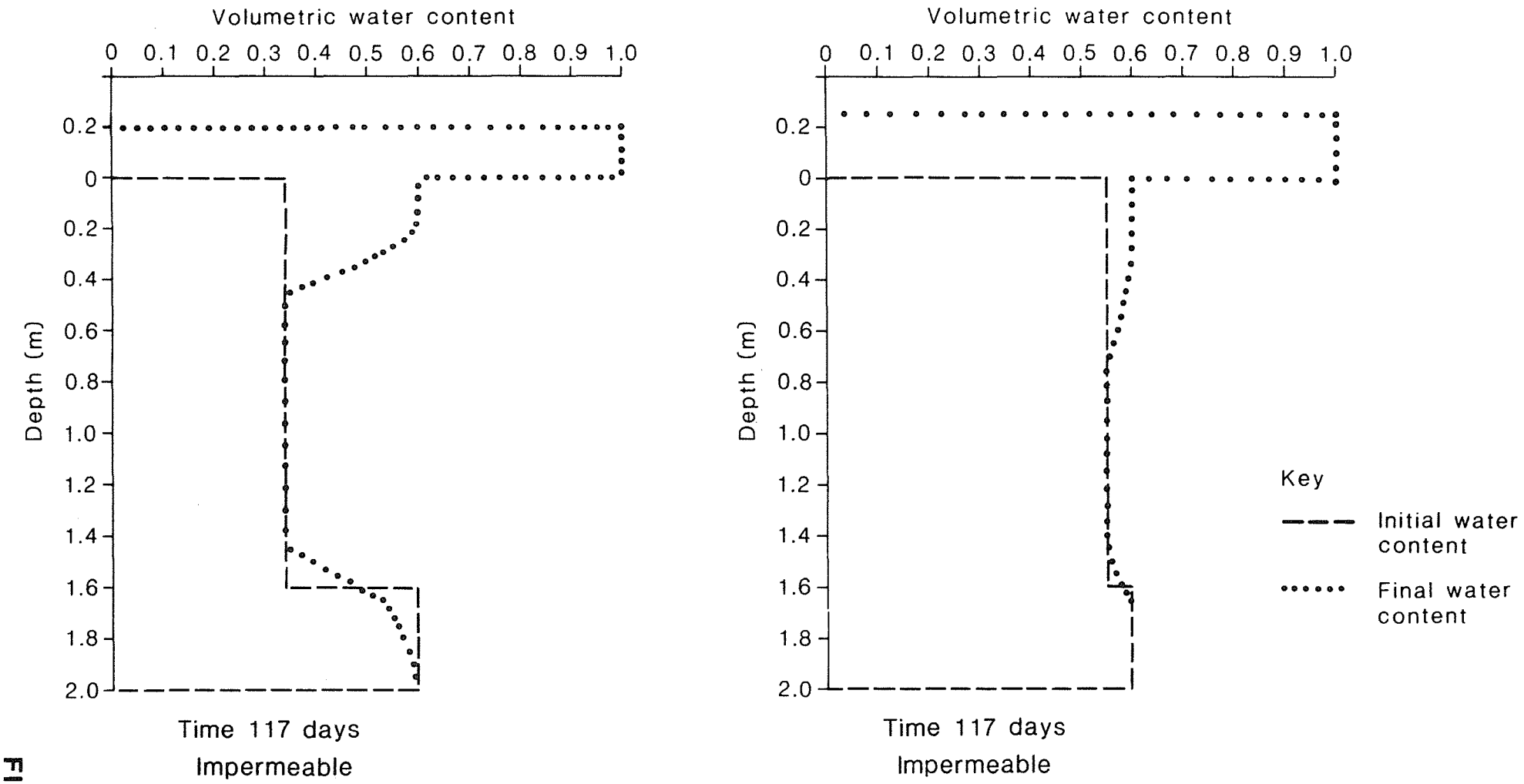

FIGURE 6

Soil water profiles following infiltration and ponding on clay

In the second example (θ_{init} = 0.55 m^3m^{-3}) the initial soil hydraulic conductivity was somewhat higher and this led to deeper infiltration. At the end of the period water had infiltrated to 0.90 m. However the total change in soil water storage was only 31 mm. This agrees with the observation that total infiltration for some soils decreases with increasing soil water content even though the initial conductivity of the soil is somewhat higher. Soil water evaporation (199 mm) equalled potential evaporation (199 mm) due to ponded water which in this case stood at 248 mm at the end of the period.

Yellow earth

Three simulations for the yellow earth soil were run with the initial conditions shown in Table 2. The resulting water content profiles are shown in Fig. 7.

In the first simulation (θ_{init} = 0.2 m^3m^{-3}), infiltrating water reached a depth of 2.1 m. Due to the high water content close to the soil surface, soil water evaporation was high (167 mm). The infiltration capacity of the soil was only exceeded during one storm during which the ponded water reached a maximum depth of 1.8 mm. The total amount of water infiltrating the soil was consequently high and an increase in soil water storage of 311 mm occurred by the end of the period.

In the second simulation, the higher initial water content resulted in faster movement of water through the soil. After only 85 mm of rain the wetting front met the redistributing wetter layer. By the end of the period nearly all of the soil profile was saturated. The soil water evaporation increased (192 mm) due to the higher water content close to the surface. On the other hand the net addition to soil water (286 mm) decreased slightly compared to the previous example.

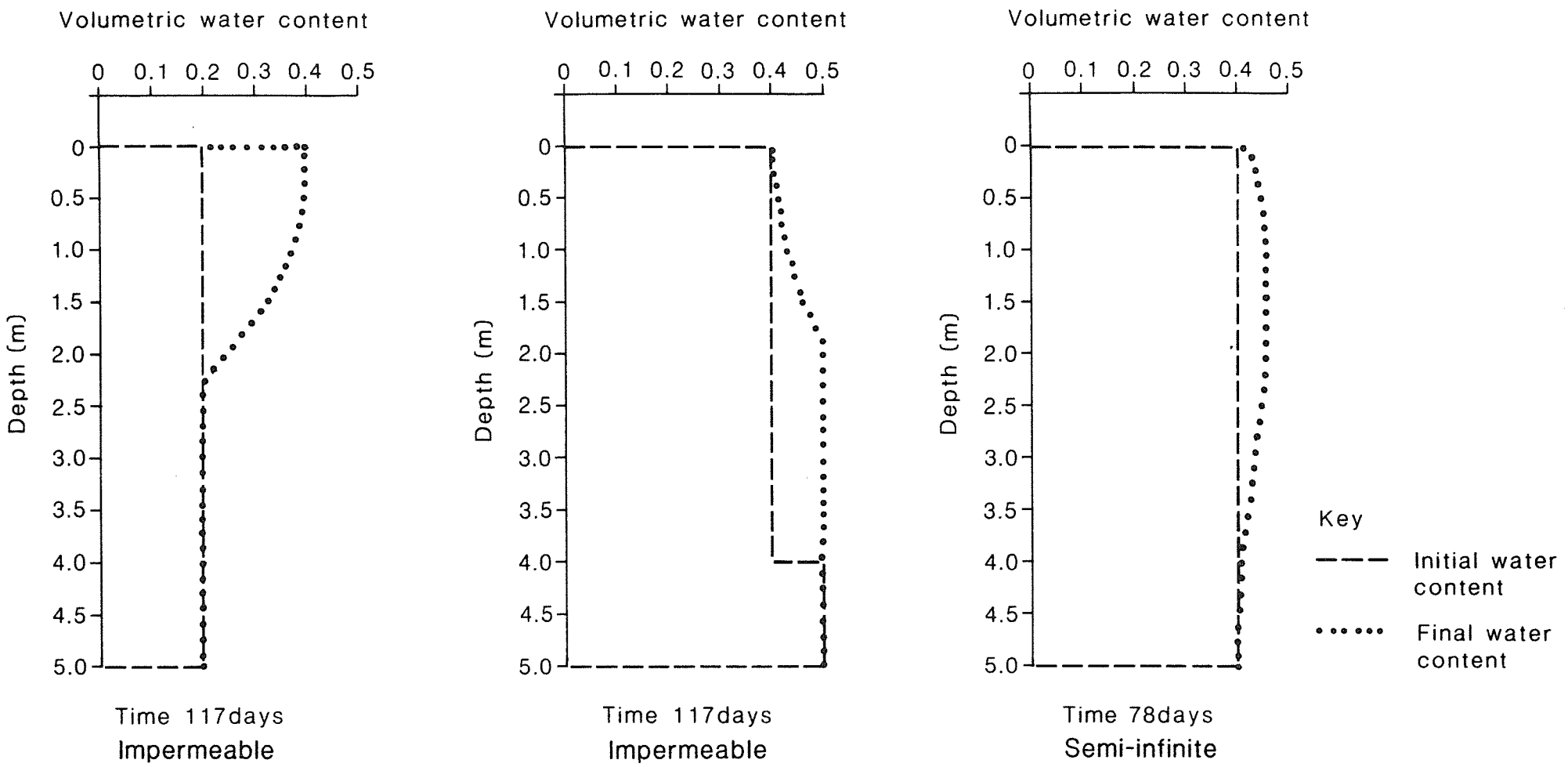

FIGURE 7

Soil water profiles following infiltration into yellow earths for various initial water profiles

In the third simulation the saturated layer was excluded. At the end of four months water had infiltrated down to 7.8 m.

Gravelly sand

This soil was the most permeable with a saturated hydraulic conductivity approaching 10 m d^{-1}. Because of this high permeability, soil water changes were much more rapid than for the other soils and this necessitated very small time-steps to maintain numerical stability when the soil approached saturation. These soils thus provided the greatest problem for seasonal simulations because of excessive computational requirements. Several methods were attempted to improve efficiency:

(i) reduce number of soil layers (N) (computational time is proportional to N^2);

(ii) increase layer thickness (this may only be useful in deep soils);

(iii) tune the parameters in the time-step criteria for optimum efficiency whilst maintaining numerical stability.

By employing the above techniques, long term simulations with minimum time-steps around 1 to 4 minutes were achieved, although computational time remained high. Five different situations were considered with the initial conditions as specified in Table 2.

The first two simulations considered infiltration for different initial water contents (Fig. 8). In the first case (θ_{init} = 0.11 m^3m^{-3}), after four months the infiltrating water had reached a depth of 4.4 m. Soil water evaporation (92 mm) was lower than that for the other soil types due to the low amount of soil water retained near the surface. The largest component of the water balance was the change in soil water storage (386 mm).

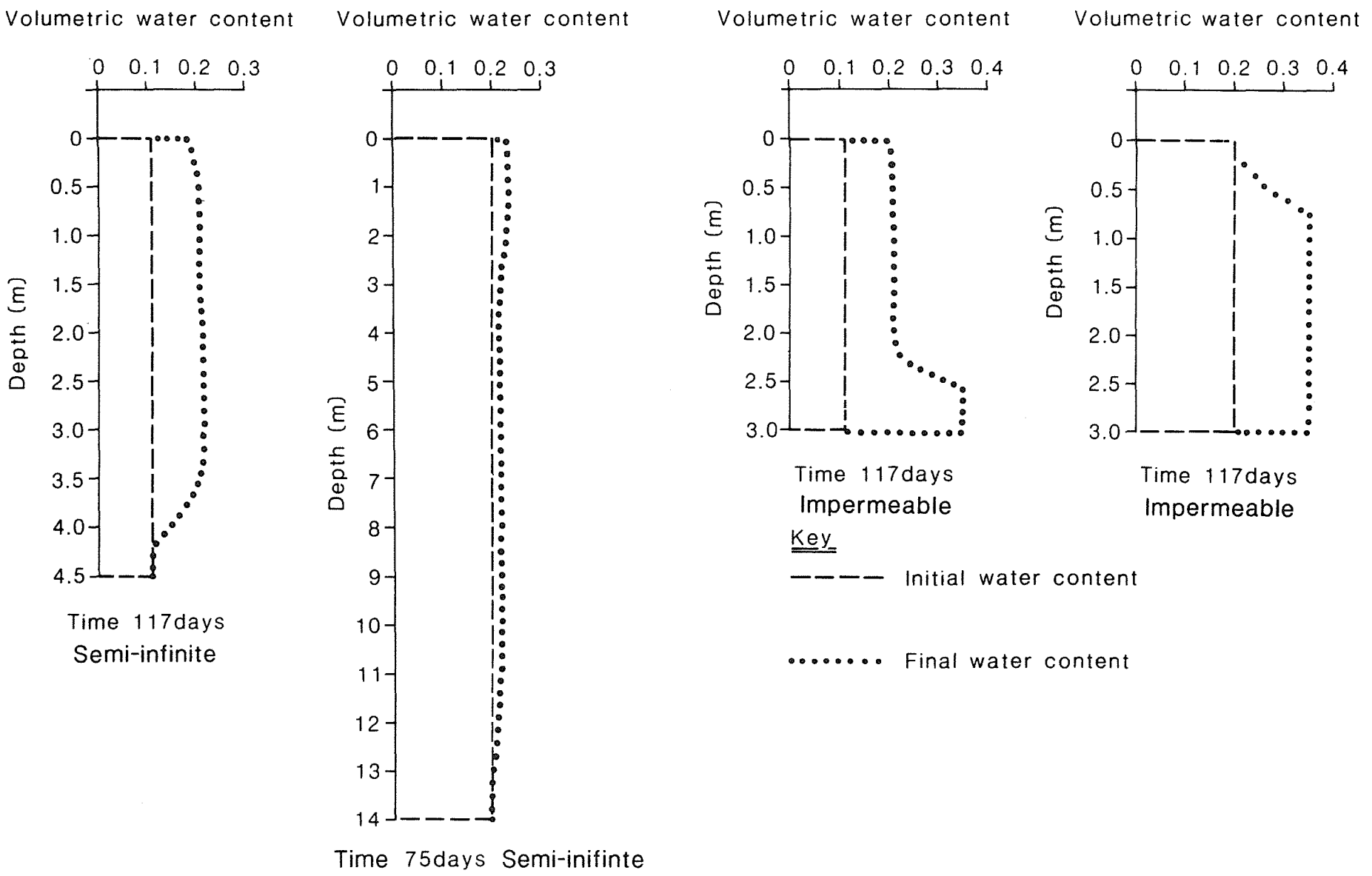

FIGURE 8

Soil water profiles following infiltration into gravelly sand for various initial water profiles

In the second example the soil water was initially at the higher value of 0.2 m^3m^{-3} and this gave rise to a rapid movement of water through the soil. After 72 days (307 mm rainfall) the infiltrating water had reached a depth of 14 m.

The next two simulations (Fig. 8) were identical to the above except that an artificial impermeable base was assumed to occur at 3 m depth. Thus once infiltrating water reached this base the soil above it became saturated. In the θ_{init} = 0.2 m^3m^{-3} example, the water table nearly reached the soil surface by the end of the period.

The above results emphasize the importance of antecedent conditions (in particular the initial water content) on infiltration, soil water evaporation and the formation of perched water tables. To obtain a more realistic initial soil water profile, the soil profile was subjected to drying from an initial water content of 0.2 m^3m^{-3} through the four month period. The resultant soil water profile was then used as the initial soil water profile in the final simulation. A generally similar result to the fourth simulation was obtained, with the water table in this case rising to 1 m below the surface.

The soil water profiles shown in Fig. 8 give little information on the relative effects of infiltration, redistribution and evaporation during the winter period. For this reason a time series of soil water profiles for the gravelly sand is illustrated in Fig. 9 (for the case θ_{init} = 0.11 m^3m^{-3}). The cycles of infiltration and redistribution following rainfall input are generally apparent with evaporation having most effect close to the surface. A summary of all the vertical model simulation results is given in Table 3.

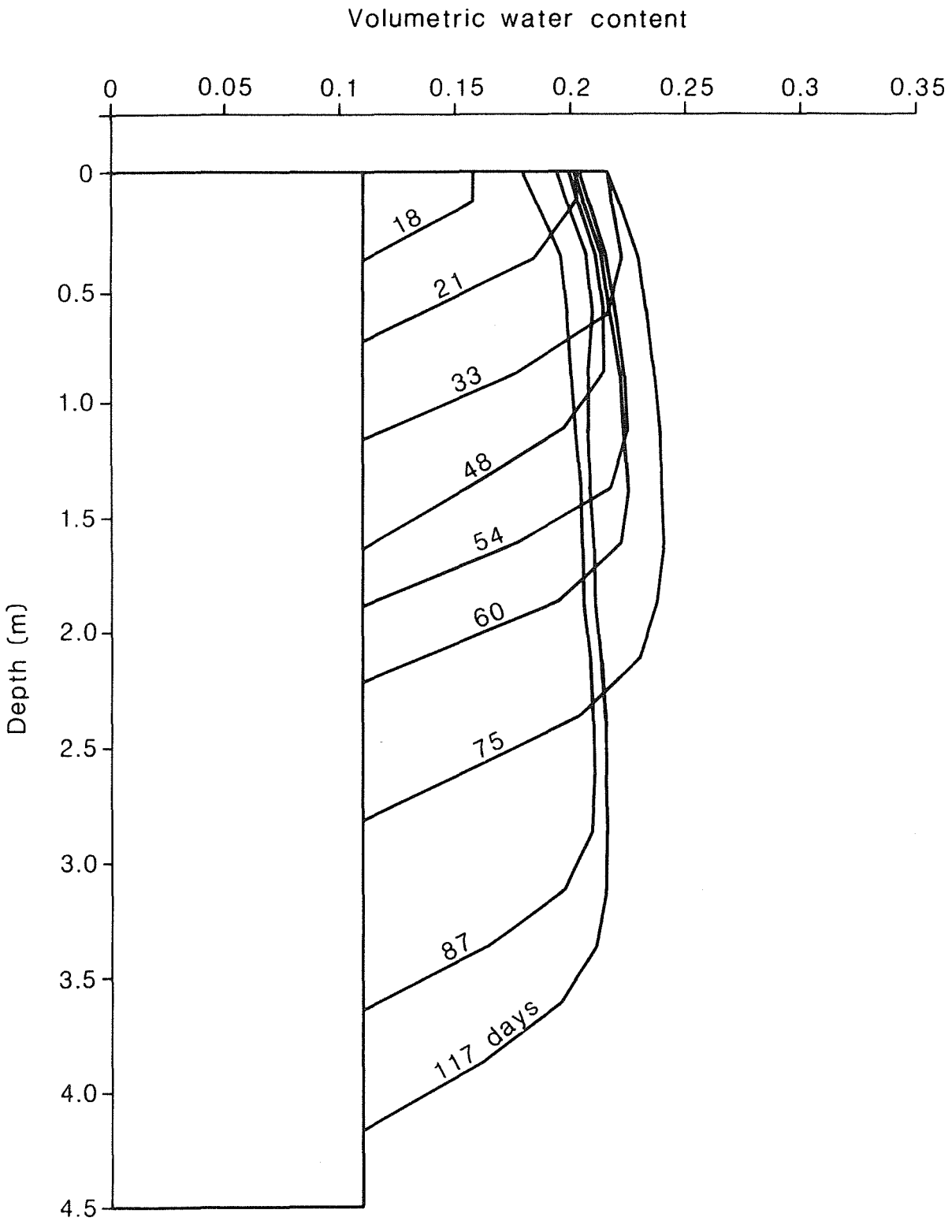

Soil water profile time series showing infiltration, redistribution and evaporation in gravelly sand

FIGURE 9

Table 3 : Vertical model results summary

Soil type	Initial water content (m^3m^{-3})	Initial depth to saturation (m)	Period (days)	Rainfall (mm)	Potential evap. (mm)	Soil water evap. (mm)	Change in soil water storage (mm)	Infiltration depth (m)	Maximum ponding (mm)	Final ponding (mm)	Minimum timestep (mins)
clay	0.34	1.6	117	478	199	190	89	0.45	205	199	180
clay	0.55	1.6	117	478	199	199	31	0.90	254	248	180
yellow earth	0.2	semi-infinite	117	478	199	167	311	2.1	6	0	63
yellow earth	0.4	4.0	117	478	199	192	286	W/T	13	0	61
yellow earth	0.4	semi-infinite	117	478	199	194	352	7.8	5	0	180
gravelly sand	0.11	semi-infinite	117	478	199	92	386	4.2	0	0	1
gravelly sand	0.20	semi-infinite	72	307	107	63	244	14.0	0	0	20
gravelly sand	0.11	3.0	117	478	199	94	384	W/T	0	0	2
gravelly sand	0.20	3.0	117	478	199	101	377	W/T	0	0	3

3. ONE DIMENSIONAL UNIFORM SLOPE MODEL

The development of a hillslope model was restricted to a single uniformly sloping element (Fig. 10). The additional processes included were overland flow and saturated throughflow. Unsaturated throughflow was not incorporated because saturated throughflow in perched aquifers is the dominant lateral flow mechanism in the region (Stokes and Loh, 1982). The model was applied to clay soil and to duplex sand over clay and yellow earth over clay soils.

3.1 Mathematical Formulation

Overland flow

A simple treatment of overland flow was employed. The surface discharge per unit width for turbulent flow is given by Manning's equation:-

$$q_s = \frac{1}{n} S^{\frac{1}{2}} H^{\frac{5}{3}} \tag{12}$$

where n is Manning's roughness factor, S is the slope and H is the depth of surface water.

Substituting into the continuity equation:

$$\frac{\partial H}{\partial t} = -\frac{\partial q_s}{\partial x} \tag{13}$$

gives

$$\frac{\partial H}{\partial t} = -\frac{S^{\frac{1}{2}} H^{\frac{5}{3}}}{n x_L} \tag{14}$$

where X_L is the horizontal length of the uniformly rough plane surface of the single element.

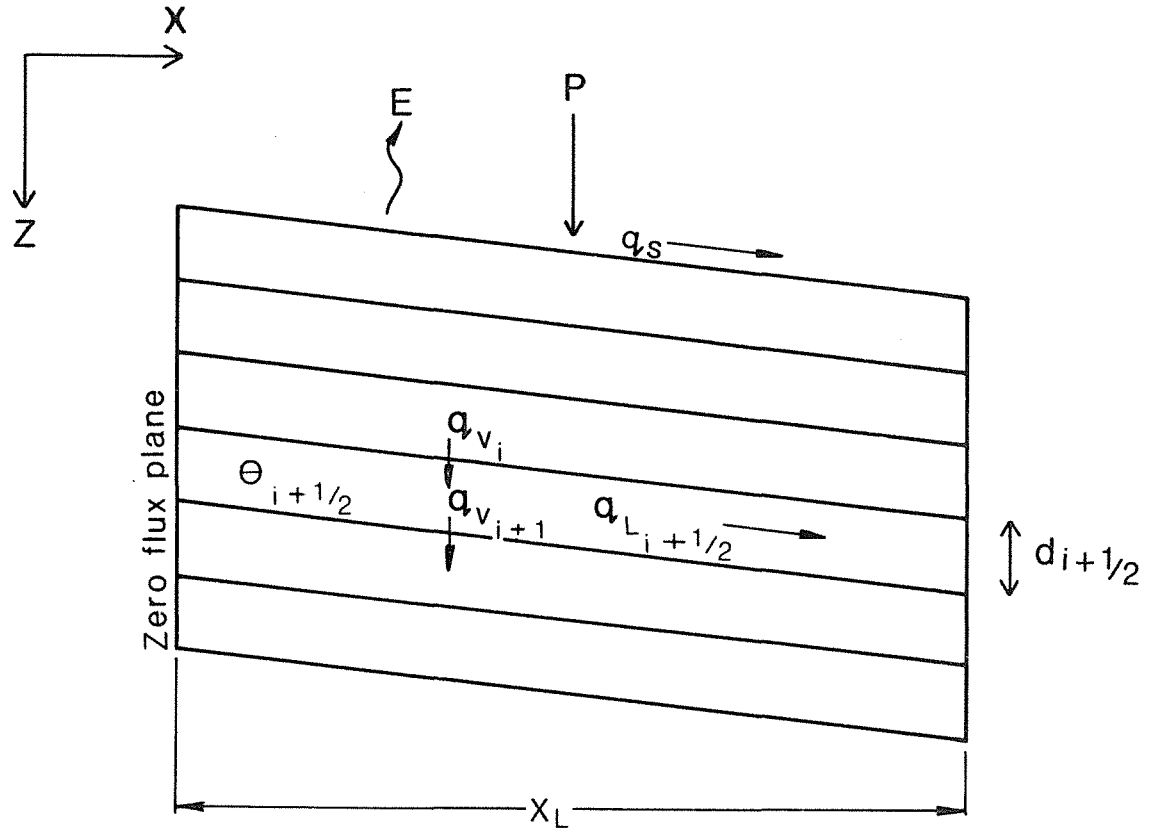

Schematic diagram of one-dimensional uniform slope model

FIGURE 10

In reality overland flow is usually partly laminar and partly turbulent and the depth exponent should lie between 1.67 and 3. Hillel (1980) suggested that an exponent of 2 gives satisfactory results and that value was adopted.

The numerical accuracy in solving the overland flow equation explicitly was ensured by introducing a further time-step criterion based on the Manning velocity (v_m):

$$\Delta t \leq \beta \, X_L / v_m \tag{15}$$

where β is an adjustable constant.

Saturated throughflow

The situation considered was the development of a perched aquifer in a sandy or loamy superficial soil overlying a clay subsoil. Saturated throughflow was simply treated as a sink term operational when any layer became saturated.

The change in soil water content with time is given by

$$\frac{\partial \theta}{\partial t} = - \frac{\partial q_v}{\partial z} - \frac{\partial q_L}{\partial x} \tag{16}$$

where q_v and q_L are the vertical and lateral fluxes respectively.

Assuming a zero flux plane exists at the upper vertical boundary of the slope element, the set of first order differential equations to be solved are

$$\frac{d\theta_{i+\frac{1}{2}}}{dt} = \frac{q_{v_i} - q_{v_{i+1}}}{d_{i+\frac{1}{2}}} - \frac{q_{L_{i+\frac{1}{2}}}}{X_L} \quad , \quad i=1, N-1 \tag{17}$$

where $q_{L_{i+\frac{1}{2}}} = - K_{sat_{i+\frac{1}{2}}} S$ (18)

and K_{sat} is the saturated hydraulic conductivity. The set of differential equations (17) were again solved simultaneously with a fourth order Runge-Kutta algorithm.

3.2 Results

Clay soil

The first simulation, for a clay soil of low permeability, generated a high proportion of surface runoff. The model parameters are listed in Table 4.

Table 4 : Model parameters for clay uniform slope simulations

slope(S)	0.02
length (x_L)	120 m
initial water content (θ_{init})	0.34, 0.55 m^3m^{-3}
Manning roughness coefficient (n)	0.1
surface velocity time-step parameter (β)	0.5
number of layers	5
thickness of layers	0.1 m
surface depression storage	2.5 mm

The results of the simulation are illustrated in Fig. 11. Of the 478 mm rainfall, 231 mm became surface runoff and a further 186 mm was evaporated, with only 60 mm infiltrating the clay soil. The second simulation, with $\theta_{init} = 0.55\ m^3m^{-3}$, produced 256 mm overland flow, 198 mm evaporation and only 21 mm infiltration.

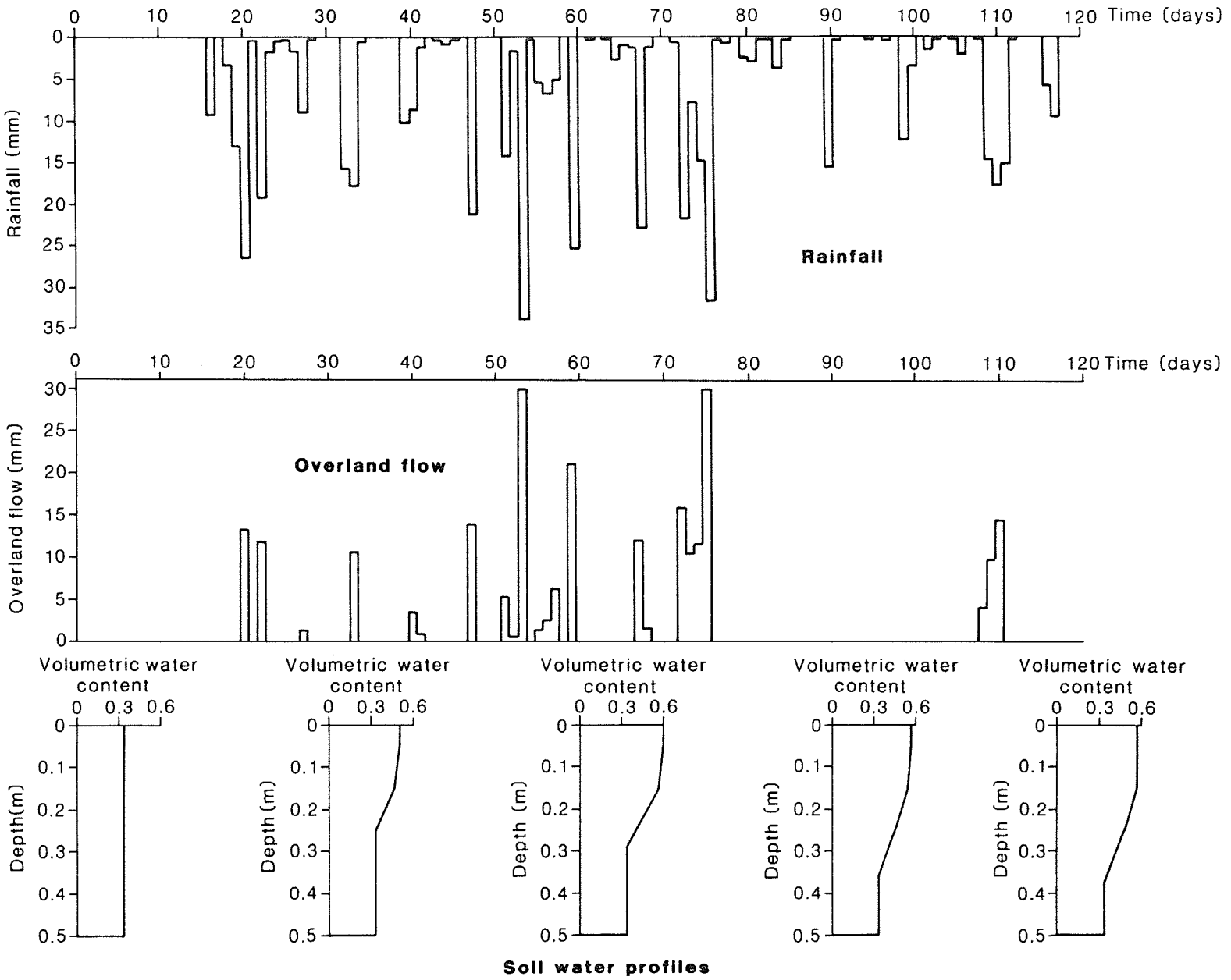

FIGURE 11

Clay uniform slope simulation showing overland flow and soil water profile responses to rainfall

Duplex soils

The model parameters for gravelly sand over clay and yellow earth over clay simulations are listed in Table 5.

Table 5 : Model parameters for duplex yellow earth over clay and gravelly sand over clay uniform slope simulations

Model Parameters	yellow earth/clay	sand/clay
slope (S)	0.088	0.088
length (x_L)	225 m	225 m
saturated conductivity (K_{sat})	4.2×10^{-5} m/min	6.7×10^{-3} m/min
initial water content (θ_{init})	0.3/0.38 m^3m^{-3}	0.11/0.39 m^3m^{-3}
roughness coefficient (n)	0.1	0.1
time-step parameter (δ)	0.5	0.5
thickness of A horizon	1.0 m	1.0 m
no. of layers in A horizon	5	4
no. of layers in subsoil	5	4
evaporation limit (θ_L)	0.2	0.1
surface depression storage	2.5 mm	2.5 mm

Yellow earth over clay

The rainfall, runoff and soil water content profiles for a simulation involving one metre of yellow earth over clay are shown in Fig. 12. The soil water content was initialised at 0.3 m^3m^{-3} in the yellow earth and 0.38 in the clay horizon. The early rainfall infiltrated the soil and after 40 days a near-uniform soil water profile close to 0.4 m^3m^{-3} had developed in the upper horizon. The heavy rainfall on the 53rd day produced a small amount (12 mm) of infiltration excess overland flow. A short time later a perched water table developed above the impeding clay horizon. Since the saturated conductivity of the yellow earth

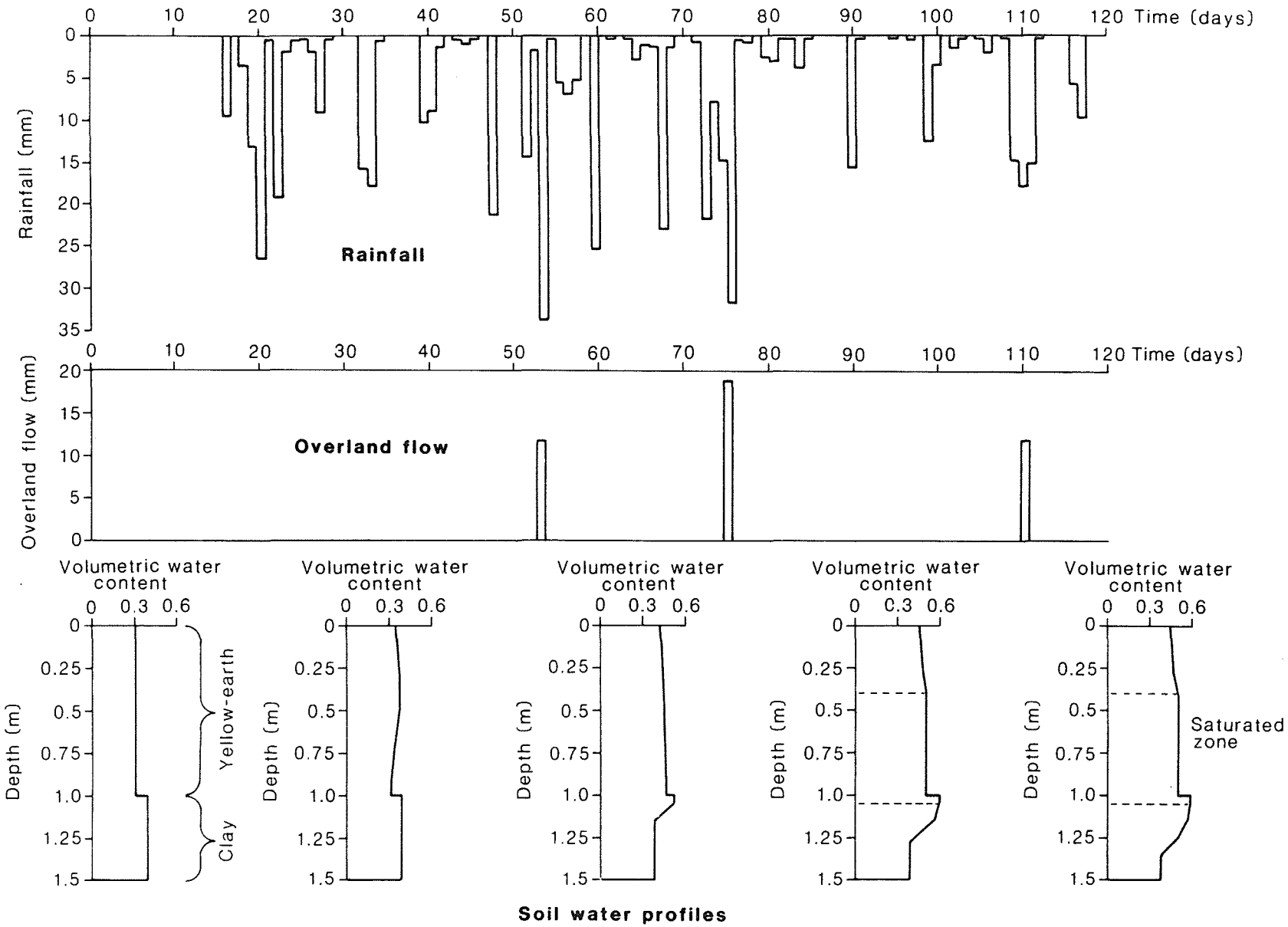

FIGURE 12

Duplex yellow earth over clay uniform slope simulation showing overland flow and soil water profile responses to rainfall

soil was low, little saturated throughflow occurred and the upper horizon soon saturated. Considerable saturation excess overland flow was generated during the 70-73 day storm period. The water table remained high to the end of the simulation period but only one further rainfall event yielded overland flow. In this simulation, 43 mm became overland flow, 197 mm was lost to evaporation, 53 mm infiltrated the clay subsoil, 185 mm became topsoil water storage and only 0.5 mm drained as saturated throughflow.

A second simulation in which the upper horizon was extended to 2 m showed a dramatic reduction in overland flow to 2 mm. This decrease was due to the increased soil water deficit of the upper horizon. Soil water deficit, whether in terms of soil water content at the end of summer, or in the depth of permeable soil, was found to be a major determinant of the amount of overland flow generated by saturation of the topsoil.

Gravelly sand over clay

Long term simulations of gravelly sand over clay were the most difficult to achieve due to the high hydraulic conductivity at or near saturation of the upper horizon. The high hydraulic conductivity enforces small time-steps to maintain the numerical stability and accuracy of the solution. This situation becomes increasingly acute with decreasing depth of upper horizon. The number of model layers through the profile was decreased to 8 to reduce computational time.

The rainfall, overland flow, saturated throughflow and soil water profiles for the simulation involving a one metre upper horizon are shown in Fig. 13. By 40 days the wetting front had reached the clay horizon and a perched water table had formed. At this stage saturated throughflow became prominent and effectively drained the perched aquifer so that very little saturation excess overland flow occurred. By the end of the simulation period,

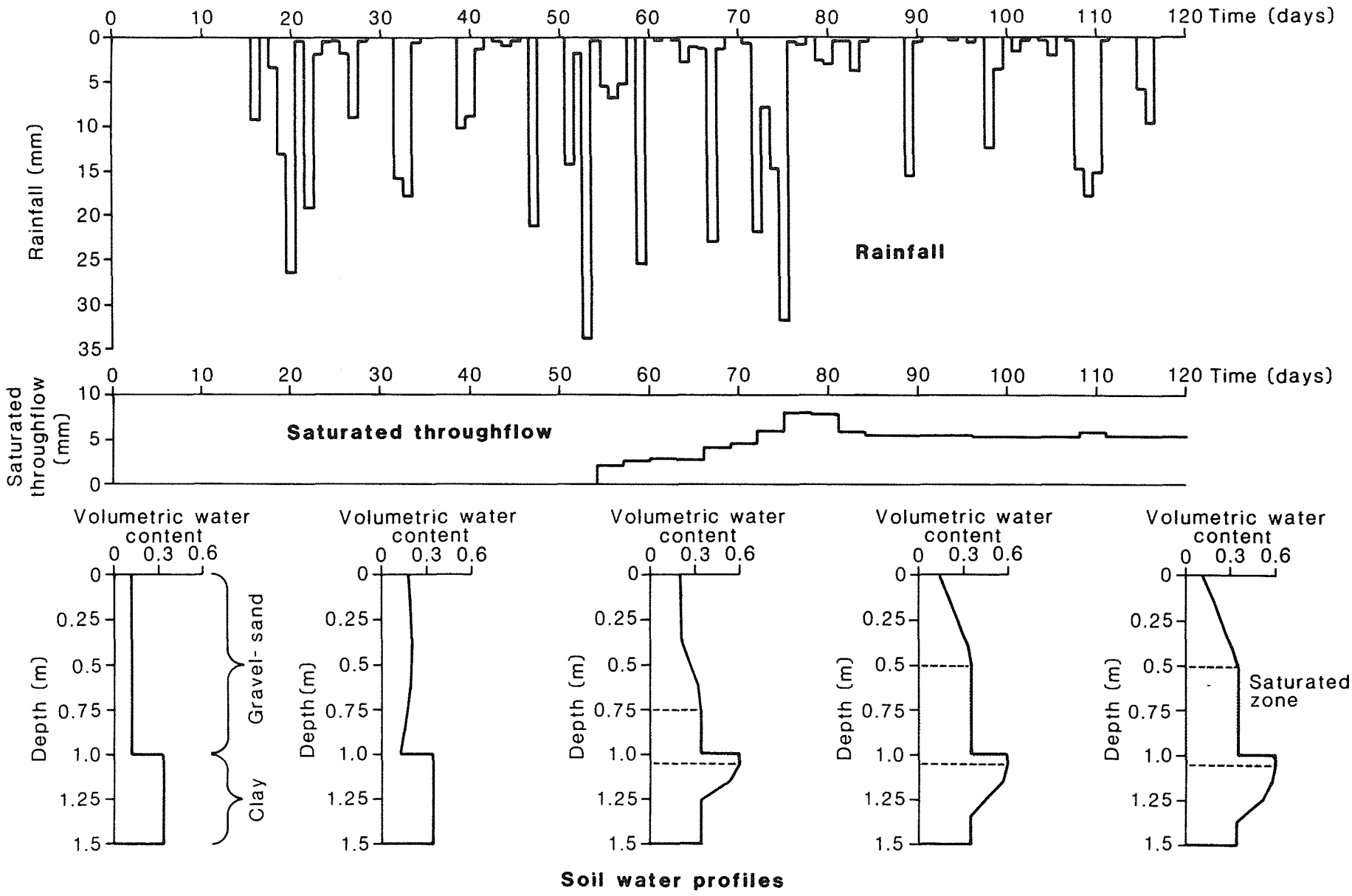

FIGURE 13

Duplex gravel-sand over clay uniform slope simulation showing saturated throughflow and soil water profile responses to rainfall

113 mm had drained as saturated throughflow, 104 mm was lost to evaporation, 189 mm had been added to topsoil water storage and 72 mm had infiltrated the clay subsoil. There was no overland flow.

A second simulation with a two metre gravelly sand upper horizon again demonstrated the effect of soil water deficit by reducing saturated throughflow to 50 mm. In this example 263 mm of the 478 mm rainfall was held in soil water storage at the end of the simulation period. A summary of the results of the simulations described above is given in Table 6.

Table 6 : Summary of uniform slope model results

Soil type	Surface soil depth	Initial water content (m^3m^{-3})	Rain (mm)	Potential evap. (mm)	Soil water evap. (mm)	Overland flow (mm)	Throughflow (mm)	Change in topsoil water storage (mm)	Maximum ponding (mm)	Final depth to water table (m)	Change in subsoil water storage (mm)
clay	-	0.34	478	199	186	231	-	60	5.0	-	-
clay	-	0.55	478	199	199	256	-	21	5.0	-	-
yellow earth/ clay	1.0	0.3/0.39	478	208	197	42.5	0.5	185	5.7	0.4	53
yellow earth/ clay	2.0	0.3/0.38	478	208	192	2.0	0.0	256	2.2	2.0	27
gravelly sand/ clay	1.0	0.11/0.34	478	208	104	0.0	113	189	0.0	0.5	72
gravelly sand/ clay	2.0	0.11/0.34	478	208	100	0.0	50	263	0.0	1.6	65

4. SUMMARY AND CONCLUSIONS

A model has been developed which is capable of estimating seasonal soil water profiles, soil water evaporation, overland flow, infiltration and saturated throughflow for one-dimensional vertical soil profiles and uniformly sloping soil profiles. The model has been applied to a range of soil types and to duplex soils.

The model was found to be numerically accurate, stable and efficient for clay and loam soils because of their low hydraulic conductivites. The model was less efficient in simulating gravelly sand due to its high hydraulic conductivity, especially at or near saturation or for a shallow soil horizon. This necessitated small integration time-steps and consequently high computer time usage. However, four-monthly simulations of a one metre gravelly sand horizon overlying clay, involving saturated throughflow, were achieved.

The one-dimensional vertical flow model was applied to three textural classes, namely clay, sandy loam and gravelly sand. Infiltration into the clay was very slow (0.4 - 0.8 m in four months) and this resulted in considerable ponding at the surface. The depth to which water infiltrated was found to increase with initial soil water content. However the amount of infiltrating water decreased with increasing initial water content which supports the field observation that for some soils infiltration capacity decreases with water content, despite the higher hydraulic conductivity.

The rate of infiltration into the sandy loam (yellow earth) was much greater than for clay and was also very sensitive to initial soil water content. The infiltration depth after 4 months ranged from 2 metres at θ_{init} = 0.2 m^3m^{-3} to 8 metres at θ_{init} = 0.4 m^3m^{-3}. Evaporation from the sandy loam was slightly less than that for clay.

Gravelly sand provided the fastest advance of the wetting front, which again was very sensitive to initial soil water content. For the case θ_{init} = 0.11 m^3m^{-3}, the wetting front had reached 4.4 metres after 4 months while for θ_{init} = 0.2 m^3m^{-3} a depth of 14 metres was attained in a little over 2 months. The fast movement of water through the soil resulted in substantially smaller evaporation losses from the gravelly sand in comparison to the other soil types.

The uniform slope model was applied to a clay soil and to duplex yellow earth over clay and gravelly sand over clay soils. In the former case, as one may expect, substantial overland flow was generated from the low permeability clay soil.

The consideration of duplex soils was of more interest to the local environment. One and two metre upper horizons for yellow earth and gravelly sand were considered. The water balance components were found to be highly sensitive to the depth of the upper horizon. In the case of yellow earth over clay, substantial overland flow occurred as a result of the upper horizon becoming saturated. One reason for the upper horizon becoming saturated was its insignificant depletion by saturated throughflow, due to the low saturated conductivity of the soil. In contrast, in the gravelly sand over clay duplex soil, significant saturated throughflow occurred in the upper horizon which in turn substantially reduced overland flow. When the depths of the upper horizons are increased, their soil water storages are increased and consequently much less water is available to saturate the upper horizon, thus causing significant decreases in overland flow and saturated throughflow.

Future work will involve the testing of the models against known analytical and numerical solutions and field experiments. In addition the inclusion of hysteresis and unsaturated throughflow will be considered.

5. ACKNOWLEDGEMENTS

Gratitude is extended to the Computing Centre of the WA Institute of Technology for running computer models on their DEC10 and to the staff of the Water Authority of W.A. Hydrology Branch for providing climatical data. The author is also most appreciative of the constructive criticisms provided by Dr A.A. Curtis (CSIRO) and Dr B.C. Bates (Water Authority of W.A.).

6. REFERENCES

Clapp, R.B. (1983). Estimating spatial variability in soil moisture with a simplified dynamic model. Water Resour. Res., 19(3), 739-745.

Dagan, G. and Bresler, E. (1983). Unsaturated flow in spatially variable fields. 1. Derviation of models of infiltration and redistribution. Water Resour. Res., 19(2), 413-420.

Hanks, R.J. and Bowers, S.A. (1962). Numerical solution of the water flow equation for infiltration into layered soils. Soil Sci. Soc. Am. Proc., 26, 530-534.

Haverkamp, R., Vauclin, M., Touma, T., Wierenga, P.J. and Vachaud, G. (1977). A comparison of numerical simulation models for one-dimensional infiltration. Soil Sci. Soc. Amer. Proc., 29, 495-504.

Haverkamp, R. and Vauclin, M. (1979). A note on estimating finite difference interblock hydraulic conductivity values for transient unsaturated flow problems. Water Resour. Res., 15(1), 181-188.

Hillel, D. (1975). Simulation of evaporation from bare soil under steady and diurnally fluctuating evaporativity. Soil Sci., 120(3), 230-237.

Hillel, D. (1980). Applications of Soil Physics, Academic Press.

Hillel, D. and Talpaz, H. (1977). Simulation of soil water dynamics in layered soils. Soil Sci., 123, 54-62.

Klute, A. (1952). A numerical method for solving the flow equation for water in unsaturated materials. Soil Sci., 73, 105-116.

Markar, M.S. and Mein, R.G. (1983). Numerical simulation of evaporation from bare soils. Hydrology and Water Resources Symposuim, Hobart, Inst. Eng. Aust. Publ. No. 83/13, 231-235.

Rubin, J. (1967). Numerical method for analyzing hysteresis - affected post-infiltration redistribution of soil moisture. Soil Sci. Soc. Am. Proc., 31, 13-20.

Saxton, K.E., Johnson, H.P. and Shaw, R.H. (1974). Modelling evapotranspiration and soil water. Trans. Amer. Soc. Ag. Eng., 17(4), 673-677.

Sharma, M.L., Williamson, D.R. and Peck, A.J. (1980). Characterization of soil hydraulic properties of a catchment. Land and Stream Salinity Seminar, Perth, Govt. Western Aust.

Stokes, R.A. and Loh, I.C. (1982). Streamflow and solute characteristics of a forested and deforested catchment pair in south western Australia. 1st Nat. Symp. For. Hydrol., Melbourne, Inst. Eng. Aust., Publ. No. 82/6, 60-66.

Vachaud, G., Vauclin, M. and Khanji, D. (1973). Effects of air pressure on water flow in an unsaturated stratified vertical column of sand. Water Resour. Res., 9(1), 160-173.

Watson, K.K. and Curtis, A.A. (1975). Numerical analysis of vertical water movement in a bounded profile. Aust. J. Soil Res., 13, 1-11.

Watson, K.K. and Lees, S.J. (1975). Simulation of the rainfall-runoff process using a hysteretic infiltration - redistribution model. Aust. J. Soil Res., 13, 133-140.

Whisler, F.D., Watson, K.K. and Perrens, S.J. (1972). The numerical analysis of infiltration into heterogeneous porous media. Soil Sci. Soc. Am. Proc., 36, 868-874.

Wind, G.P. and Van Doorne, W. (1975). A numerical model for the simulation of unsaturated vertical flow of water in soils. J. Hydrol., 24, 1-20.

APPENDIX I : Runge-Kutta algorithms to solve water transport equations

The Runge-Kutta algroithm is a self-starting, multi-step method derived from a Taylor series expansion. The order of the method for solving an ordinary differential equation is defined as the number of terms needed in the Taylor series for the same accuracy. The fourth order method is used here and is described in the following.

Consider the differential equation

$$\frac{dy}{dx} = f(x,y)$$

To solve this differential equation, i.e. to find the value of y for a particular x, given the value of y at the initial point, the region is divided into subintervals of width w and the following iteration is performed:

$$y_{j+1} = y_j + 1/6\ (k_1 + 2k_2 + 2k_3 + k_4)$$

where

$$k_1 = f(x_j, y_j)w$$

$$k_2 = f(x_j + 1/2w, y_j + 1/2k_1)w$$

$$k_3 = f(x_j + 1/2w, y_j + 1/2\ k_2)w$$

$$k_4 = f(x_j + w, y_j + k_3)w$$

The method is multi-step because it uses points at $x = x_j$, $x = x_j + 1/2w$ and $x = x_j+w$, yet because it generates its own intermediate steps it is self-starting.

The soil water equation for the vertical model is

$$\frac{d\theta}{dt}_{i+\frac{1}{2}} = \frac{q_i - q_{i+1}}{d_{i+\frac{1}{2}}} \quad , \quad i = 1, N-1$$

or

$$\frac{d\theta}{dt}_{i+\frac{1}{2}} = \frac{K_i(\theta)}{d_{i+\frac{1}{2}}} \left[\frac{h_{i-\frac{1}{2}} - h_{i+\frac{1}{2}}}{0.5(d_{i-\frac{1}{2}} + d_{i+\frac{1}{2}})} \right] - \frac{K_{i+1}(\theta)}{d_{i+\frac{1}{2}}} \left[\frac{h_{i+\frac{1}{2}} - h_{i+1\frac{1}{2}}}{0.5(d_{i+\frac{1}{2}}+d_{i+1\frac{1}{2}})} \right]$$

$$= f(\theta,h)$$

Substituting into the Runge-Kutta iteration:

$$\theta_{i+\frac{1}{2}}(t+\Delta t) = \theta_{i+\frac{1}{2}}(t) + \frac{1}{6}(k_1 + 2k_2 + 2k_3 + k_4)$$

where

$$k_1 = f_1(\theta,h)\Delta t$$

$$k_2 = f_2(\theta',h')\Delta t$$

where $\theta' = \theta + \frac{1}{2}k_1$

$$k_3 = f_3(\theta'',h'')\Delta t$$

where $\theta'' = \theta + \frac{1}{2}k_2$

$$k_4 = f_4(\theta''',h''')\Delta t$$

where $\theta''' = \theta + k_3$.

An identical procedure is followed in the sloping model where the soil water transport equation takes the form:

$$\frac{d\theta}{dt}_{i+\frac{1}{2}} = \frac{q_{v_i} - q_{v_{i+1}}}{d_{i+\frac{1}{2}}} - \frac{q_{L_{i+\frac{1}{2}}}}{x_L} \quad , \quad i=1, N-1$$

In this case there is simply an extra term in the function evaluations.

APPENDIX II Adjustment of climatical input data to variable time increments

When using a variable time-step in the solution of the differential equations, it is necessary to convert the climatical data input, which is on a fixed time increment, to the new computed time-step. Different algorithms are necessary for doing this depending on whether the computed time interval lies within an input time-increment or whether it crosses the boundary. These two situations are discussed below:

(a) Time-step lying within input time interval

This situation is illustrated below. If t_1 is

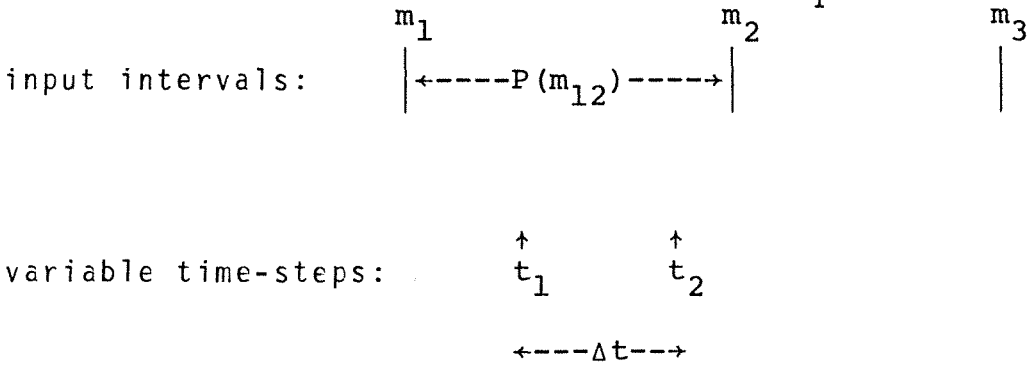

the time at the end of the previous time-step and Δt is the computed time-step, then the time at the end of this new time-step is

$$t_2 = t_1 + \Delta t$$

If Δt lies between the input time-intervals m_1 and m_2 and $P(m_{12})$ is the climatical quantity associated with this interval, then the value of the climatical variable for the time-step Δt is:

$$P(\Delta t) = (t_2 - t_1)\, P(m_{12})$$

(b) Time-step traversing input time-interval boundary

This situation is illustrated below. If f_1 is the fraction

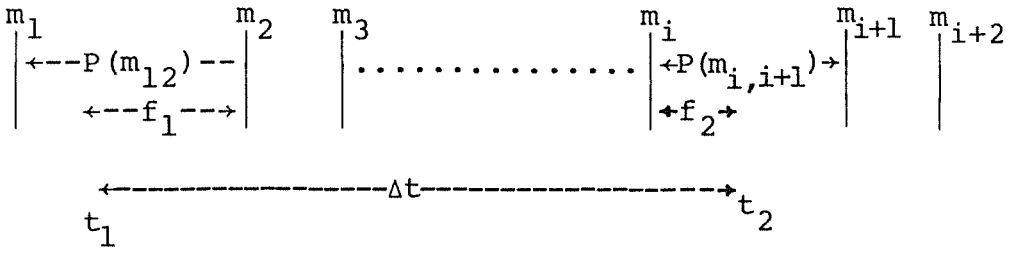

of $P(m_{12})$ in Δt and f_2 is the fraction of $P(m_{i,i+1})$ in Δt, then the value of the climatical variable for the time-step Δt is

$$P(\Delta t) = \sum_{i=m_2}^{i=i-1} P(m_i) + f_1\, P(m_{12}) + f_2\, P(m_{i,i+1})$$

where

$$f_1 = m_2 - t_1$$

$$f_2 = t_2 - m_i$$